JOURNAL OF PROPULSION AND POWER
Vol. 23, No. 2, March–April 2007

Effects of Equation of State and Transport on Pulsed Plasma Accelerator Modeling

J. T. Cassibry*
University of Alabama, Huntsville, Alabama 35899

DOI: 10.2514/1.22890

Various equations of state and transport models were used in the study of the time and spatial evolution of the magnetic field in a high power, parallel rail geometry, pulsed plasma thruster. Comparisons were made between magnetic field measurements in the experimental data and modeling results. Assessments are made about the appropriateness of the equation of state and transport models used in this study. The most significant finding was that the calorically perfect assumption of the ideal gas model led to an overestimate of the plasma temperature and consequently, frozen-in, stationary fields at the breech. Marked improvement in agreement between experimental and modeling data was observed with the use of a tabular equation of state model which accounted for multiple ionization states and electronic excitation modes. Agreement was less sensitive to various transport models.

Nomenclature

B	=	magnetic field, T
Cv	=	constant volume specific heat, J/kg · K
d	=	active electrode width along z, m
f	=	curve fit function for Braginskii thermal conductivity
I	=	current, A
k	=	thermal conductivity, W/m · eV
P	=	pressure, Pa
T	=	temperature, eV
x	=	axial coordinate, m
y	=	transverse coordinate, m
Z	=	effective charge
η_D	=	electrical diffusivity, m^2/s
λ	=	coulomb logarithm
μ_0	=	magnetic permeability (H/m)
ρ	=	mass density, kg/m^3
τ	=	collision time, s
Ω	=	Hall parameter
ω	=	gyrofrequency, 1/s

Subscripts

e	=	electron
z	=	out of plane coordinate, m

Introduction

PULSED electromagnetic plasma thrusters (PEPT) have potential as energy efficient (∼60%) [1] in-space propulsion systems with high specific impulse (>2000 s) [2] and thrust densities (10^4–10^5 N/m^2, theoretical). To assess the ability of a 2-D resistive magnetohydrodynamic (MHD) code to predict trends in these devices, it is beneficial to study the sensitivity of the code to various equation of state and transport models. In this way, one can have at least a qualitative understanding of the limitations of those models when applied to PEPTs.

Presented as Paper 2361 at the 35th AIAA Plasma Dynamics and Lasers Conference, Portland, OR; received 31 January 2006; revision received 26 April 2006; accepted for publication 31 July 2006.

*Assistant Research Professor, Propulsion Research Center, Department of Mechanical and Aerospace Engineering, Technology Hall S-227. Member AIAA.

Other authors have performed sensitivity studies on similar devices. York et al. [3] investigated acceleration of a plasma through a magnetic nozzle generated by a theta pinch coil. They required a factor of 10 times the classic thermal conductivity in order for their 1-D MHD model to match the spatial electron temperature profile in the experiments. Marklin and Frese [4] investigated field reversed configuration (FRC) formation. The peak density and temperature reached were moderately sensitive to the anomalous resistivity model used. Mikellides [5] performed simulations of a megawatt-class, self-field magnetoplasmadynamic (MPD) thruster. The electron-neutral collision contributed significantly to electron scattering; thus the classic Spitzer resistivity model was inadequate for capturing current distributions.

In this research note, various equations of state and transport models are used in the study of the time and spatial evolution of the magnetic field in a high-power, parallel rail geometry, pulsed plasma thruster. The objective is to qualitatively assess the usefulness of these models in PEPT problems of interest. To the author's knowledge, this type of study has not been formerly discussed in the literature for PEPTs, and should be of value to those with an interest in modeling such devices.

In the next section, the numerical model based on the experimental apparatus is discussed. A description of the current sheet evolution is given, followed by an analysis of the discrepancies between the model and experiment in which current sheet velocities from the model are compared with the experimental measurements. Assessments are made about the appropriateness of the equation of state and transport models used in this study.

Numerical Model

The parallel rail geometry pulsed electromagnetic accelerator investigated experimentally by Markusic and Choueiri [6,7] and more recently by Berkery and Choueiri [8,9] was chosen for this study. Berkery and Choueiri have reported among the most detailed measurements of current sheet evolution to date for a pulsed device of this type. They have measured the magnetic field at 432 spatial locations as shown in Fig. 1. The experiment consists of a pair of 60 cm long, 15 cm wide copper plates, with a 5 cm gap between the plates. Initial conditions of 100 mtorr prefill argon driven by PFN II pulse forming network [6] charged to 9 kV were chosen for the model in accordance with experimental data that have been discussed in the literature [8]. Additionally, argon is likely to demonstrate behavior under which the calorically perfect (ideal) gas assumption becomes inadequate due to multiple ionization states and numerous electronic excitation modes of the plasma species.

Based on its history of success in modeling a wide variety of physics problems, the tool for modeling the experiments presented

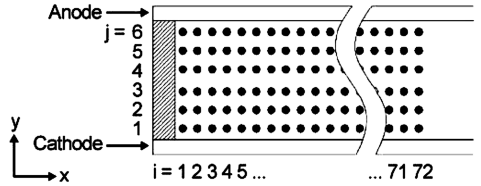

Fig. 1 Spatial location of magnetic field measurements [8].

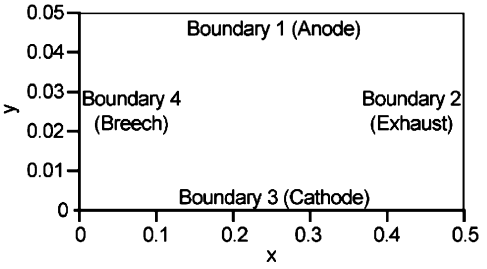

Fig. 2 Computational domain for the parallel plate geometry.

here was the 2-D MHD code MACH2 [10]. MACH2 (multiblock arbitrary coordinate hydrodynamic) is a 2-D multiblock, arbitrary Lagrangian Eulerian (ALE), resistive, single fluid MHD code that carries all three spatial components of vectors, but allows no quantity to depend on the coordinate that is normal to the computational plane. MACH2 solves the mass, momentum, electron energy, ion energy, radiation energy density, and magnetic induction equations in a fractional time-split manner for the flow variables.

The computational domain is based on the experiment as shown in Fig. 2. The domain ends at 50 cm, because magnetic field measurements are not taken beyond 46 cm. This will not affect the results, because the flow is supersonic and super-Alfvenic when the current sheet (and magnetic field) reach the exit.

Boundary 4 is treated as an insulator, and is attached to a piecewise linear current model with a pulse shape designed to emulate PFN II charged to 9 kV, Fig. 3. The equation for the magnetic field along this boundary is derived from Ampere's Law, assuming the field is uniform between the plates and neglecting the displacement current. For a parallel plate geometry, this equation is

$$B_z = \frac{\mu_0 I}{d} \tag{1}$$

where B_z is the magnetic field normal to the x–y plane of Fig. 2, μ_0 is the permeability of free space, I is the current, and d, measured along z between the insulators, is the effective acceleration width of the electrodes. Based on the experimental apparatus [6,8], d= 10.16 cm. A discussion of the remaining boundary conditions can be found elsewhere [11].

In the model, gradients in the z-direction are assumed to be zero. The fringe fields and the boundary layers at the insulating side walls are among the most important physical processes neglected with this assumption. The weaker field at the wall and the viscous drag combine to slow the plasma in this region. The dimensions of the experimental apparatus were chosen based on successful configurations of earlier researchers, partly to minimize spatial nonuniformities. Photographic evidence seems to indicate a predominately uniform current sheet along z, giving confidence in the 2-D assumption of the model [4].

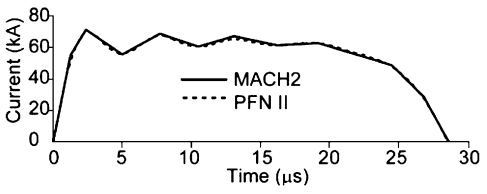

Fig. 3 Experimental [6] and numerical pulse shape.

Table 1 Summary of cases investigated using MACH2

Case	Equation of state	Electrical diffusivity	Thermal conductivity
1	Tabular[a]	Eq. (2) (Spitzer)	Eq. (6)
2	Ideal gas	Eq. (2) (Spitzer)	Eq. (6)
3	Tabular	550 $m^2/2$ (constant)	Eq. (6)
4	Tabular	Eq. (2) (Spitzer)	Eq. (3)

[a]"Tabular" refers to the tabular model for argon assuming chemical equilibrium.

Approach

Four cases were investigated in which the equation of state and transport coefficient models were varied, Table 1. Case 1 used a tabular equation of state [12], Spitzer resistivity model [13], and Braginskii formula for the thermal conductivity in the limit of high electron Hall parameter [14]. The other three cases are to be compared with Case 1. In Case 2, the equation of state was replaced with the ideal gas model. The ideal gas model requires substantially less computational time per physics cycle. Similarly, the constant resistivity model in Case 3 requires no calculation of resistivity for individual fluid elements, although appropriate values must be chosen a posteriori. Finally, the default Braginskii model is less expensive computationally and much simpler to program, but gives incorrect values when the Hall parameter is below 10.0. The full model may be necessary in some cases in a plasma accelerator, where the Hall parameter can vary from more than 100 in the vacuum field behind the current sheet to 0 downstream from the plasma jet.

For the ideal gas (calorically perfect) model, a constant specific heat ratio of 1.1 and molecular weight of 39.948 kg/kmol were used. The specific heat ratio is based on an average value using the more precise tabular model, give the experimentally determined 1–3 eV temperature range. A hydrogenlike Saha model for singly ionized argon was used with an ionization potential of 15.76 eV. The tabular equation of state model for argon was generated using a tabular equation of state model (Aurora) [12], including all 18 levels of ionization, and where available, up to 10 electronic excitation levels. The atomic data were taken from Moore [15]. This equation of state was verified against a separate table reported by Sparks and Fischel [16]. Within their range of densities and temperatures, the models agreed to within 1%. A comparison of the equations of state shows that the tabular model departs ideal gas behavior around 1 eV, Fig. 4. Additionally, the constant volume specific heat, which is constant in the ideal gas model, is low by an order of magnitude when the temperature is sufficiently high to populate an electronic excitation state, Fig. 4.

In the constant resistivity case, it was assumed that the diffusivity is 550 m^2/s, based on ~5 times the Spitzer diffusivity for a charge state of 1.0 and experimentally determined electron temperature of 2.4 eV [8]. The factor of 5 was chosen to mimic anomalous resistivity behavior. The Spitzer diffusivity is given by

$$\eta_D = 1.0328 \times 10^{-4} \frac{Z\lambda}{\mu_0 T_e^{3/2}} \tag{2}$$

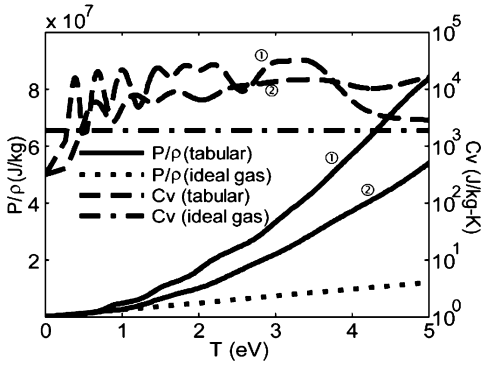

Fig. 4 Tabular and ideal gas equations of state for argon. 1) density = 10^{-6} kg/m^3; 2) density = 10^{-2} kg/m^3.

The full expression for the electron thermal conductivity is [14]

$$k_{\perp e} = \frac{9.6958 \times 10^3 T_e^{5/2}}{Z\lambda}\left(\frac{f_1\Omega_e^2 + f_0}{\Omega_e^4 + f_3\Omega_e^2 + f_2}\right) \tag{3}$$

where λ is the Coulomb logarithm, and Z is the charge state of the plasma, and T_e is the electron temperature in eV.

$$\Omega_e = \omega_e\tau_e = \frac{5.5127 \times 10^{-8}}{n_e Z^2\lambda}\frac{BT_e^{3/2}}{m_e} \tag{4}$$

The coefficients are approximated by curve fits to the values in Table 1 of Braginskii [14].

$$\begin{aligned} f_0 &= 11.92\left(0.10067 + \frac{0.58456}{-0.35 + Z^{1.1}}\right) \\ f_1 &= 4.664\left(0.69683 + \frac{0.30317}{Z}\right) \\ f_2 &= 3.7703\left(0.025489 + \frac{0.63343}{-0.35 + Z^{3/2}}\right) \\ f_3 &= 14.79\left(0.50588 + \frac{0.40765}{-0.175 + Z}\right) \end{aligned} \tag{5}$$

The simplified expression, appropriate for $x \gg 1$ is

$$k_{\perp e} = \frac{9.6958 \times 10^3 T_e^{5/2}}{Z\lambda}\frac{f_1}{\Omega_e^2} \tag{6}$$

The full expression was used only in Case 4.

Results and Discussion

In Cases 1, 3, and 4, the current sheet starts at the breech and advances uniformly downstream to a velocity of ~30 km/s. The accelerated plasma moves as a rectangular slab, growing in thickness as neutral gas is entrained by the current sheet, Fig. 5. It is important to note that unlike the experiment, the current sheet does not cant in the model, which was anticipated. Canting is believed to be caused by enhanced field penetration along the anode surface, which is a departure from ideal fluid behavior [6,17]. The canting leads to a high effective permeability in the current sheet. As a result, Berkery measured a minimum electron density of $\sim 3 \times 10^{21}$ m^{-3} immediately following the current sheet (see [9], Fig. 4.7, p. 61), where the model gave $\sim 3 \times 10^{19}$. The permeability leads to a faster current sheet (less entrained mass) with increased magnetic field dissipation in the wake compared with the numerical model. Figure 6 shows this for probe (1,1), along the row closest to the breech. The magnetic field in MACH2 for Cases 1, 3, and 4 agree fairly well with the data until about 2.5 μs, when the experimental field begins to decrease. Results from Case 2 indicate that the magnetic flux is mostly trapped at the breech. The decrease in experimental magnetic field at 2.5 μs could be due to a restrike in the arc discharge at the breech, in which the magnetic flux is partially trapped, similar to the results from Case 2.

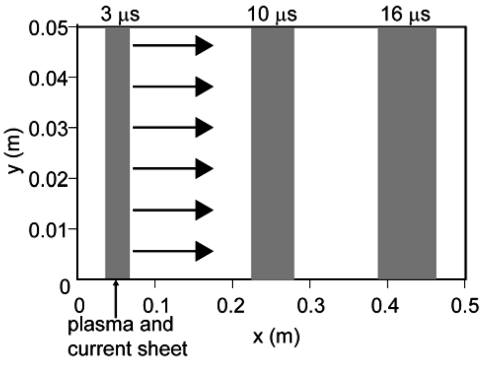

Fig. 5 Thickness and position of current sheet at 3, 10, and 16 μs.

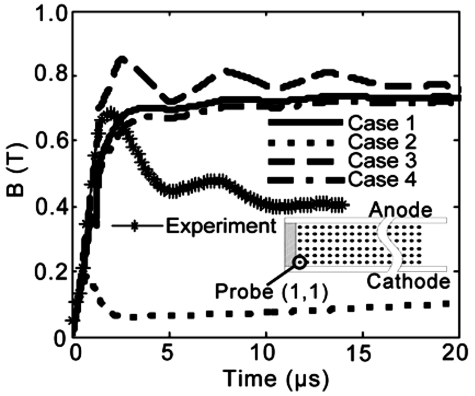

Fig. 6 Experimental and MACH2 magnetic field vs time for probe (1,1).

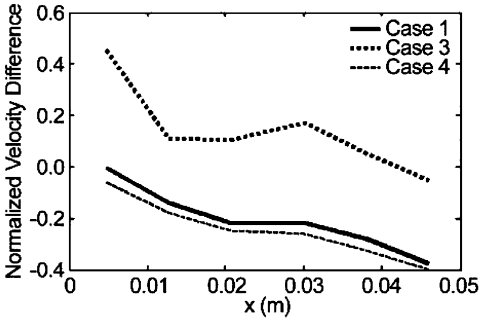

Fig. 7 Sum of normalized velocity differences at axial stations vs axial position.

The discrepancy between the model and the experiment can be quantified by comparing the velocities of the current sheet. Berkery and Choueiri interpreted the rise of the measured magnetic field from 0.0 to 0.2 T as the arrival of the current sheet at the point where the field was measured [8]. The velocity was calculated by dividing the spatial distance between adjacent magnetic field probes by the interpreted arrival time. The normalized difference in velocity between the experiment and the model is then $(v_{\text{exp}} - v_{\text{MACH2}})/v_{\text{exp}}$ at a given axial location and time. This was calculated as a function of position for each of the cases at the time of arrival of the current sheet, averaged across each row (fixed x-position).

The averaged values are plotted vs the x-axis (desired flow direction) for Cases 1, 3, and 4 in Fig. 7. For Cases 1 and 4, the results are very similar, showing that the more precise thermal conductivity model does not improve agreement with experimental data. In both cases, the agreement with the experimental data is better closer to the breech, before the effects of canting dominate the flow. Initially, the constant resistivity model (Case 3) gives a 40% higher velocity than in the experiment, but the difference improves to 10–20% downstream. The Spitzer cases (Cases 1 and 4) are within 5% initially; however, agreement worsens monotonically downstream. This suggests a transition from classic to anomalous magnetic field diffusion early in the current sheet propagation.

Case 2, which uses the calorically perfect ideal gas model, is not shown, because the current sheet did not advance beyond the breech. The cause for this is the calorically perfect gas assumption, in which the specific heat is too small, resulting in exceedingly high temperatures roughly a factor of 100 over that of the experiment. The high temperature reduces the electron scattering cross section used in the Spitzer model, making the diffusion time into the plasma long compared with the current pulse width.

Conclusions

It was observed that replacing the full Braginskii thermal conductivity model with a simplified version does not qualitatively influence current sheet motion. Current sheet velocity was best

captured by the Spitzer diffusivity model early in the numerical run, but the anomalous constant resistivity case gave better results downstream, suggesting a transition from classic to turbulent transport of the magnetic flux. The internal electronic excitation and multiple ionization states of argon captured by the tabular equation of state used in Cases 1, 3, and 4 were important in calculating the heat capacity. The calorically perfect assumption of the ideal gas model led to an overestimate of the plasma temperature and consequently, frozen-in, stationary fields at the breech. Future modeling efforts involving high power pulse plasma thrusters should include multiple ionization states in the equation of state model, if applicable. Current sheet propagation seems to be less sensitive to transport of magnetic field and heat flux, permitting some flexibility for choice of the model.

Acknowledgments

This research was funded by the Propulsion Research Center at the University of Alabama in Huntsville. The author would like to thank Jack Berkery for providing us with magnetic field probe measurements. The author would also like to thank S. T. Wu and Tom Markusic for their valuable insights.

References

[1] Gloersen, P., Gorowitz, B., and Kenney, J. T., "Energy Efficiency Trends in a Coaxial Gun Plasma Engine System," *AIAA Journal*, Vol. 4, No. 3, 1966, pp. 436–441.

[2] Cheng, D. Y., "Application of a Deflagration Plasma Gun as a Space Propulsion Thruster," *AIAA Journal*, Vol. 9, No. 9, 1971, pp. 1681–1685.

[3] York, T. M., Jacoby, B. A., and Mikellides, P. G., "Plasma Flow Processes Within Magnetic Nozzle Configurations," *Journal of Propulsion and Power*, Vol. 8, No. 5, 1992, pp. 1023–1030.

[4] Marklin, G. J., and Frese, M. H., "Field Reversed Configuration Formation Simulations with MACH2," Air Force Research Laboratory, AFRL-DE-TR-2001-1001, Albuquerque, NM, Dec. 2000.

[5] Mikellides, P. G., "Modeling and Analysis of a Megawatt-Class Magnetoplasmadynamic Thruster," *Journal of Propulsion and Power*, Vol. 20, No. 2, 2004, pp. 204–209.

[6] Markusic, T. E., "Current Sheet Canting in Pulsed Electromagnetic Accelerators," Ph.D. Dissertation, Dept. of Mechanical and Aerospace Engineering, Princeton Univ., Princeton, NJ, 2002.

[7] Markusic, T. E., and Choueiri, E. Y., "Photographic, Magnetic, and Interferometric Measurements of Current Sheet Canting in a Pulsed Plasma Accelerator," AIAA Paper 2001-3896, July 2001.

[8] Berkery, J. W., and Choueiri, E. Y., "Characterization of Current Sheet Evolution in a Pulsed Electromagnetic Accelerator," International Electric Propulsion Conference, Paper IEPC-03-307, March 2003.

[9] Berkery, J. W., "Current Sheet Mass Leakage in a Pulsed Plasma Accelerator," Ph.D. Dissertation, Dept. of Mechanical and Aerospace Engineering, Princeton Univ., Princeton, NJ, 2005.

[10] Peterkin, R. E. J., Frese, M. H., and Sovinec, C. R., "Transport of Magnetic Flux in an Arbitrary Coordinate ALE Code," *Journal of Computational Physics*, Vol. 140, No. 1, Feb. 1998, pp. 148–171.

[11] Cassibry, J. T., Thio, Y. C. F., Markusic, T. E., and Wu, S. T., "Numerical Modeling of a Pulsed Electromagnetic Plasma Thruster Experiment," *Journal of Propulsion and Power* (to be published).

[12] Cassibry, J. T., "Numerical Modeling Studies of a Coaxial Plasma Accelerator as a Standoff Driver for Magnetized Target Fusion," Ph.D. Dissertation, Dept. of Mechanical and Aerospace Engineering, Univ. of Alabama, Huntsville, AL, 2004.

[13] Spitzer, L., Jr., *Physics of Fully Ionized Gases*, 2nd ed., Interscience, New York, 1962.

[14] Braginskii, S. I., "Transport Processes in a Plasma," *Reviews of Plasma Physics*, edited by M. A. Leontovich, Vol. 1, Consultants Bureau, New York, 1965, pp. 205–311.

[15] Moore, C. E., *Atomic Energy Levels*, Vol. 1, U. S. Government Printing Office, Washington, D.C., 1949.

[16] Sparks, W. M., and Fischel, D., "Partition Functions and Equations of State in Plasmas," NASA Goddard Space Flight Center, NASA SP-3066, Washington, D.C., 1971.

[17] Peters, B., "Magnetic Field Penetration and Enhanced Diffusion in Pulsed Plasma Thrusters," M.S. Thesis, Dept. of Mechanical and Aerospace Engineering, Univ. of Alabama, Huntsville, AL, 2005.

E. Choueiri
Associate Editor